Scale-resolving simulations of laminar-to-turbulent transition in swept-wing flow

Marie Denison*, Anirban Garai†, and Scott Murman‡
NASA Ames Research Center, Moffett Field, CA 94035

I. Introduction

Aerodynamic shape optimization of swept Natural Laminar Flow (NLF) wing design plays an important role for the development of future energy-efficient commercial transport aircraft [1]. Lack of predictive laminar-to-turbulent transition modeling capabilities is still limiting the extent to which design can rely on computational tools, while making costly wind tunnel and flight tests a necessity. Prediction of transition on practical 3D wing geometries using the e^N method coupled with laminar boundary layer and linear stability codes [2, 3] or local statistical correlation CFD models such as the $\gamma - Re_\theta$ Langtry-Menter model [4] have proven challenging [5, 6], whereas transitional hybrid RANS-LES solvers have shown encouraging but still mitigated results [7–9].

Transition over swept wings has been studied using linear and non-linear Parabolized Stability Equations (PSE) mostly with surface roughness [10–14]. These stability modeling efforts were able to predict some of the dominant stationary and traveling crossflow modes and sometimes the location of transition in presence of roughness elements. Ref. [15] reported LES simulations of an infinite swept Chernoray C16 aerofoil on which a stationary vortex packet was generated by continuous suction on the surface. The results were considered qualitative only due to grid under-resolution. In Ref. [16] DNS was used in the transition region of an infinite NLF swept wing to study high-frequency secondary instabilities of stationary crossflow vortices excited by instability waves injected at the inlet. Within the single-wavelength span studied, the wall shear distribution was found to show the sawtooth pattern characteristic for crossflow transition. Nishino and Shariff [17] as well as Templemann [18] performed larger-scale Direct Numerical Simulations (DNS) in a domain covering the leading edge and upper surface of an NLF(2)-0415 infinite swept wing for the study of the boundary layer receptivity to surface roughness as experimentally characterized by Saric and Reibert [19, 20]. Nishino and Shariff used a 6^{th}-order compact finite difference scheme on a staggered grid in space and a 2^{nd}-order fully-implicit Beam-Warming scheme for the time integration. Up to 48 degrees of freedom (DOF) were used per stationary crossflow vortex wavelength. The amplitude of the steady crossflow modes was found to be more than an order of magnitude smaller than that measured in the experiments, possibly the result of lacking resolution, roughness, or freestream disturbance effects. Templemann used a spectral finite element method with finer grid, in which the lower wing part and the leading-edge region were not accounted for in the simulation of the perturbed flow. The simulation was able to resolve strong crossflow vortices, but the predicted modal amplitude was still 40% of that measured at $Re_c = 2.4 \times 10^6$, which was conjectured to result from experimental uncertainties. In Ref. [21], Butler and Wu studied the stationary crossflow vortices near the leading edge of three-dimensional boundary-layers and showed that stationary crossflow vortices have a viscous and non-parallel genesis near the leading edge that is neglected in most analyses (including PSE) but can have a leading-order effect on the initial growth rate of the crossflow disturbances.

The capability to quantitatively predict the different stages of external flow transition on a realistic geometry with extended region of laminar flow, from the onset and growth of Tollmien-Schlichting (TS) and crossflow modes to secondary instabilities and three-dimensional turbulent breakdown has thus yet to be demonstrated. Although computationally expensive, scale-resolving simulations can provide valuable insights to inform and improve RANS and LES wall models through detailed studies of the mechanisms driving transition and the build-up of validation data bases. In the present work, scale-resolving simulations of transition over an infinite swept wing are performed and validated against the experiments conducted by Dagenhart and Saric on a smooth 45-degree swept NLF(2)-0415 wing [22]. We investigate the resolution and flow perturbations required to capture the dominant stationary and traveling crossflow

*NASA Advanced Supercomputing Division, marie.f.denison@nasa.gov.
†Science and Technology Corporation, anirban.garai@nasa.gov.
‡NASA Advanced Supercomputing Division, scott.m.murman@nasa.gov.

modes and transition front features. The simulations are carried out with a fully implicit solver based on a high-order space-time spectral-element discontinuous-Galerkin (DG) algorithm. The following section provides details on the flow solver. Section III describes the selected flow conditions, wing geometry and coarse grid used to start the study. Section IV summarizes the initial results, followed by an outline of the workplan for the final paper.

II. Numerical method

The solver is based on a high-order space-time spectral-element discontinuous-Galerkin (DG) algorithm with an entropy stable formulation [23–25]. It utilizes numerical methods and linear algebra kernels that were optimized to exploit current and projected HPC capabilities, making the code highly efficient and scalable [24, 26, 27]. The entropy-stable scheme of Ismail and Roe [28] is used for the inviscid fluxes, whereas viscous fluxes are computed using an interior penalty method with parameter based on Bassi and Rebay [29]. It was validated up to 16^{th} spacial and temporal order with highly separated turbulent flows [30, 31]. Integrals are approximated by the Gauss-Legendre-Lobatto quadrature rule using twice as many quadrature points as solution points to reduce aliasing errors and increase stability when evaluating non-linear products. The element order in space and time can be varied over the domain and building blocks have been put in place for *h-p* adaptivity [32]. The solver is particularly adequate to tackle the present HPC challenge which is to perform resolved transition simulations of an external aerodynamic case at moderate Reynolds number.

III. Case set-up

The experiments by Dagenhart and Saric were conducted in the Arizona State University Unsteady Wind Tunnel [22]. In the test section the liners at the ends of the 45° swept NLF(2)-0415 wing were designed to emulate the path of streamlines in free air and simulate an infinite swept-wing flow. The largest part of the experimental data relates to the case at $\text{Re} = 2.37 \times 10^6$ based on the streamwise chord length $c = 1.83$m and $\alpha = -4°$, and was therefore selected for this study. The simulated Mach was set to 0.1, close to the maximum wind tunnel velocity of 36 ms^{-1}. The upper velocity range was selected because we use a compressible solver without pre-conditioning. Table 1 summarizes the wing geometry and modeled flow conditions.

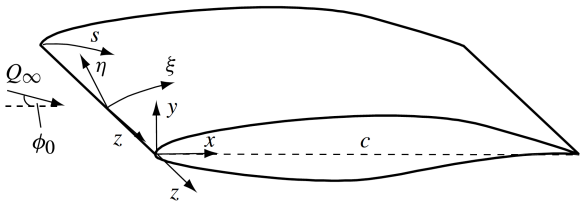

Fig. 1 Sketch of a section of the NLF(2)-0415 infinite swept wing [22]. C **is the un-swept chord length. The experiments are scaled with respect to the streamwise chord length** $c = 2/\sqrt{2}C = 1.83$ m**. The leading edge is oriented at an angle of** $\phi_0 = 45°$ **with respect to the freestream flow** Q_∞**.**

Table 1 Geometry and flow conditions

Feature	Value
Airfoil	NLF(2) − 0514
Span S/c	0.141
Sweep angle ϕ_0	45°
Reynolds number $\text{Re}_c = \frac{u_\infty c}{\nu_\infty}$	2.37×10^6
Mach number M_∞	0.1
Angle of attack α	−4°
Temperature	288.15 K

A coarse C-grid was run as a starting point to set up the simulation and post-processing workflow. The domain

extends by about 50 chord units around the airfoil. The grid includes 49×10^3 8^{th}-order elements or 25×10^6 DOF. The wall normal element distribution was defined for a maximum viscous grid spacing of $y^+ = 1.5$ at the wall in the turbulent region. The number of elements in the boundary layer increases from 2 at the leading edge to 6 in the wake. Based on the experiments, the crossflow vortices are expected to be oriented at an angle of circa 5° from the streamwise direction, with a spanwise wavelength of $\lambda/\mathrm{c} = 4 \times 10^{-3}$. The grid includes 16 elements in the spanwise direction and is therefore expected to cover about 2 vortex wavelengths per element. The streamwise resolution is increased downstream of $\mathrm{x/c} = 0.35$. The simulation was run with 4^{th} order in time and a time step of 1×10^{-3}T where T is the time it takes for the flow to travel one chord length. Statistical solution averaging was started at t=50 T.

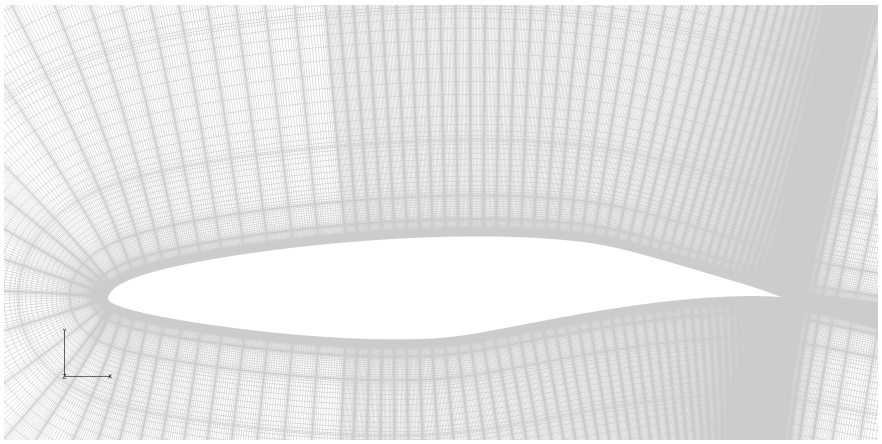

Fig. 2 Close-up of the initial coarse grid around the wing at $\mathrm{z/c} = 0$**.**

IV. Results

Numerical simulation results using the previously described computational set-up predicts that transition occurs at $x/c = 0.78$ with a uniform spanwise front, Fig. 3. Weak crossflow vortices are observed prior to transition (Fig. 5). In the experiment, the transition location was determined from the abrupt shift in sublimation rate of the naphthalene coating due to turbulence-induced shear stress increase. Transition occured at an average of $x/c = 0.58$ with a series of overlapping turbulent wedges forming a saw-tooth pattern (Fig. 4(a)), which was suggested to originate from small variations in the surface finish near the leading edge of the model [33]. For these same flow conditions the simulations results are closer to the $Re = 1.93 \times 10^6$ case in terms of transition location and front shape, Fig. 4(b). In this image one can notice regularly spaced streaks nearly parallel to the inviscid flow direction that are characteristics of crossflow vortices. The simulation results agree well with the measurements in the laminar boundary layer over the first quarter of the upper surface (Fig. 6). Further downstream, the crossflow develops in the form of skewed, counter-rotating vortices, Fig. 7. The crossflow wavelength projected in the direction of the leading edge sweep $\lambda/\mathrm{c} = 5$mm is smaller than the measured value of 6.2 mm. The crossflow vortices are oriented at 12° with respect to the freestream direction (Fig. 5), compared with 5° in the experiments. At $x/c = 0.55$, the simulated stationary cross flow amplitude is three orders of magnitude lower than in the experiments, Fig. 8.

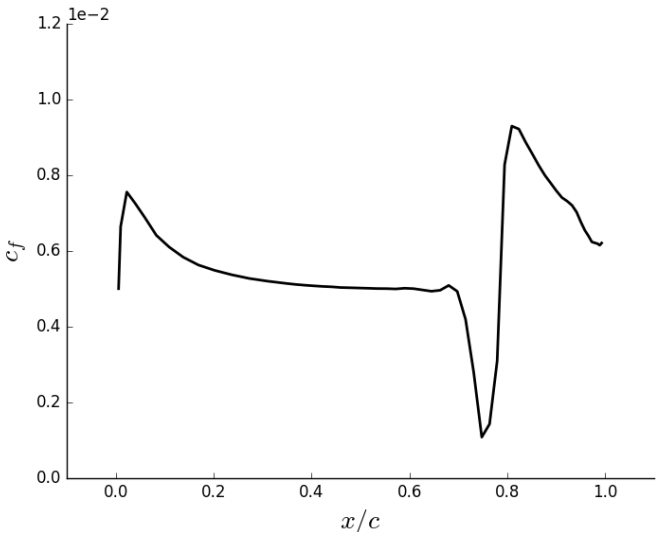

Fig. 3 Friction coefficient on the upper side of the wing.

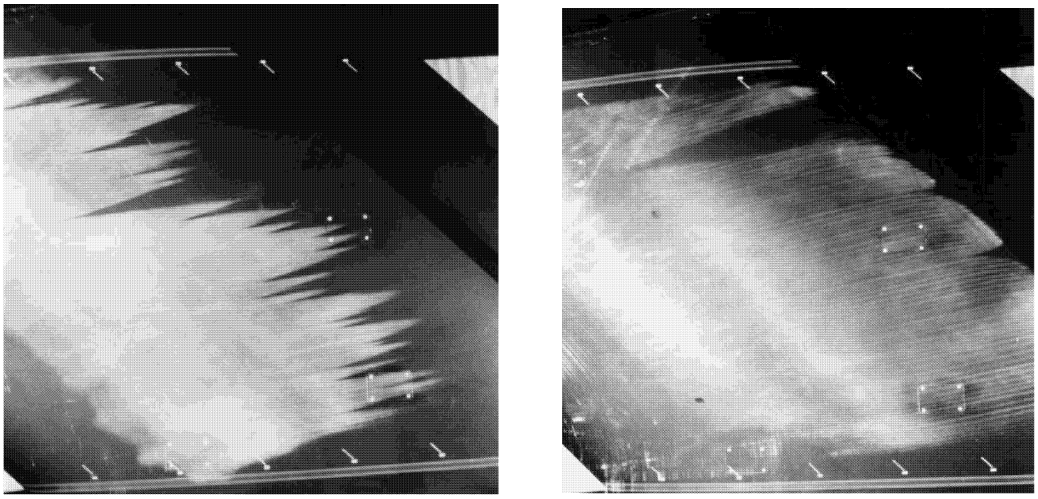

(a) $Re = 2.4 \times 10^6$ (b) [$Re = 1.93 \times 10^6$

Fig. 4 Naphtalene flow visualization at $\alpha = -4^\circ$ [22].

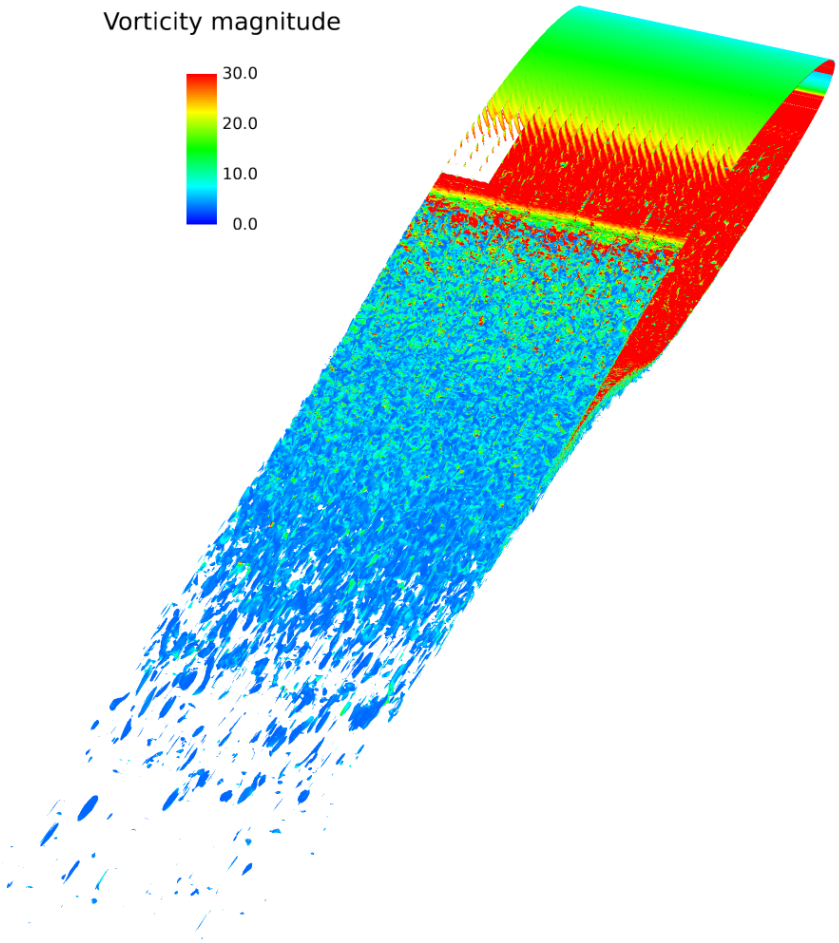

(a) Isocontours of streamwise vorticity ($\omega_x = 3\ s^{-1}$).

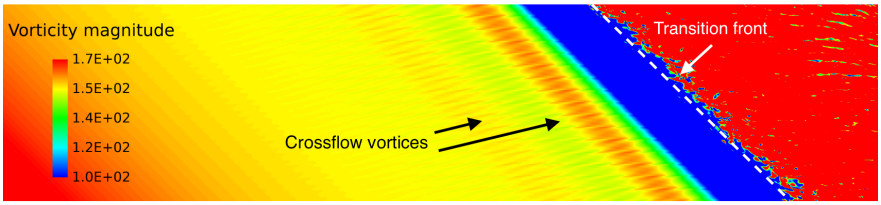

(b) Isosurface of vorticity magnitude at $y/c = 8 \times 10^{-4}$ (top view).

Fig. 5 Contours of vorticity magnitude.

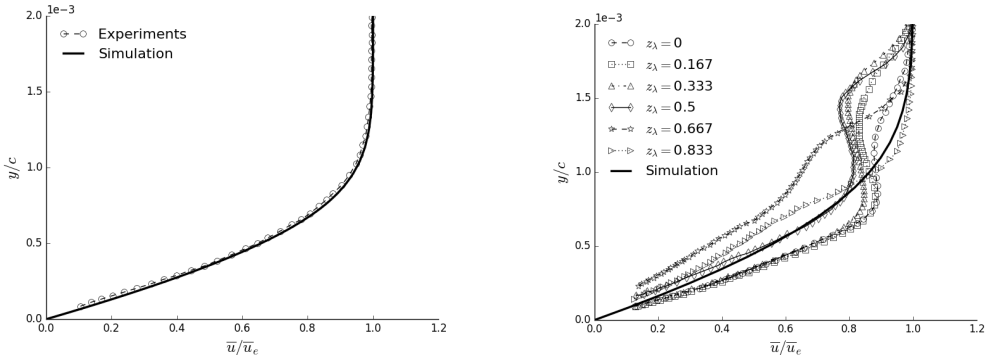

(a) $x/c = 0.25$ (b) $x/c = 0.55$

Fig. 6 Laminar streamwise velocity profile compared to experiments (symbols) [22]. (a) At $x/c = 0.25$, the perturbations are of small amplitude and only the sweep-wise span-averaged velocity is shown. (b) At $x/c = 0.55$, experimental profiles at different spanwise stations along the wing sweep are shown. Only one simulation curve is shown since the amplitude of the perturbations would be indistinguishable at this scale.

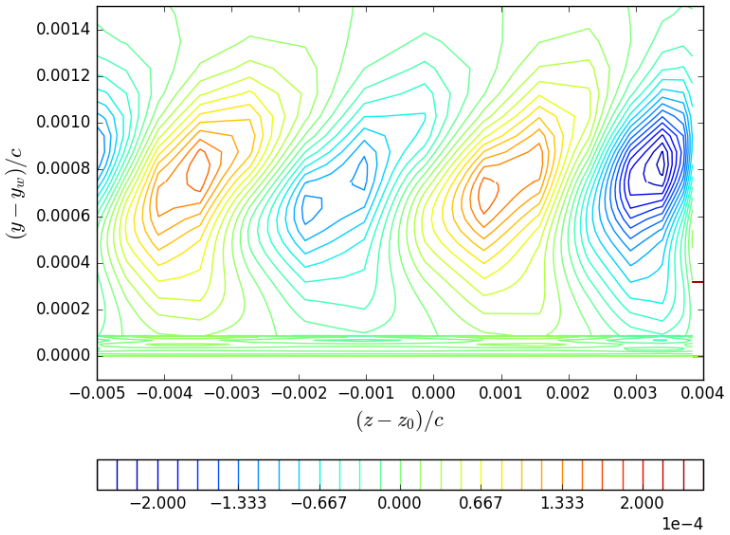

Fig. 7 Contours of streamwise velocity perturbation in a plane parallel to the wing leading edge passing through the point $x/c = 0.55,\ z/c = 0$.

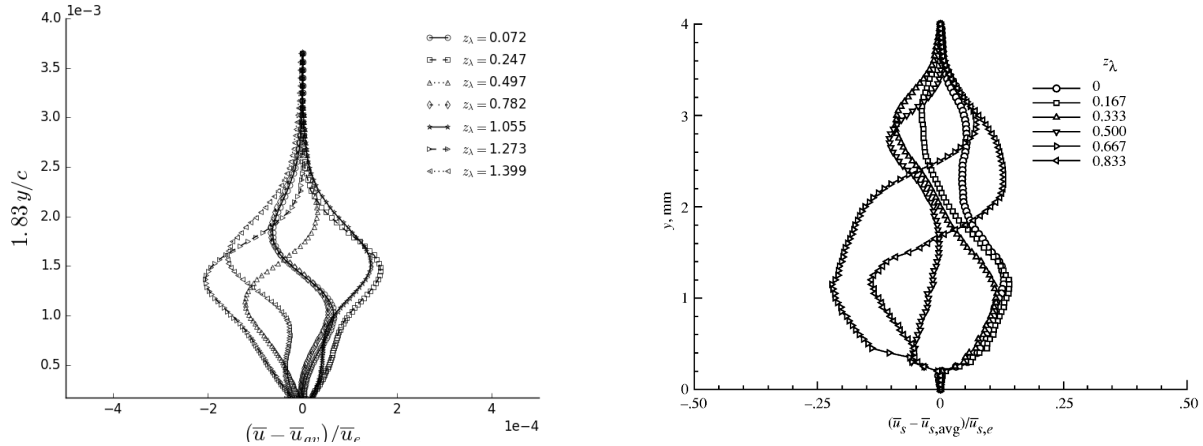

(a) Simulation with y-axis scaled by the experimental chord length of 1.83m.

(b) Experiments [22]

Fig. 8 Streamwise velocity perturbations $(\overline{u}-\overline{u}_{av})/\overline{u}$ at different coordinates along a line parallel to the leading edge passing through the point $x/c = 0.55,\ z/c = 0$.

The above results clearly indicate that the initial coarse grid does not resolve the onset and growth of the disturbances responsible for transition. A refined grid was generated to improve the resolution of the TS and crossflow modes in the forward part of the wing. As our initial focus is to explore the resolution and boundary conditions necessary to reproduce the experiments, the spanwise width of the domain is set to 5 crossflow wavelengths in this grid iteration. The spanwise resolution is increased from 8 to 40 DOF per wavelength in the laminar region. The constant wall-normal grid refinement was replaced by a streamwise-growing layer based on a Falkner-Skan profile along the upstream portion of the wing. There is a minimum of 4 elements in the boundary layer at $x/c = 0.1$ where the stability theory reported in Ref. [22] indicated a peak in stationary crossflow growth rate. A Spalding profile was used to control the growth of the wall-normal refinement beyond the point of experimental transition with $y^+ < 1$ at the wall. A buffer layer of variable stretching rate is used between the near wall and farfield regions to smooth the grid distribution. The domain was partitioned to use 8^{th}-order near the wall, gradually decreasing to 2^{nd} order in the farfield. The mesh includes 8×10^5 elements of which 2×10^5 are 8^{th}-order elements, with a total of 123×10^6 DOF.

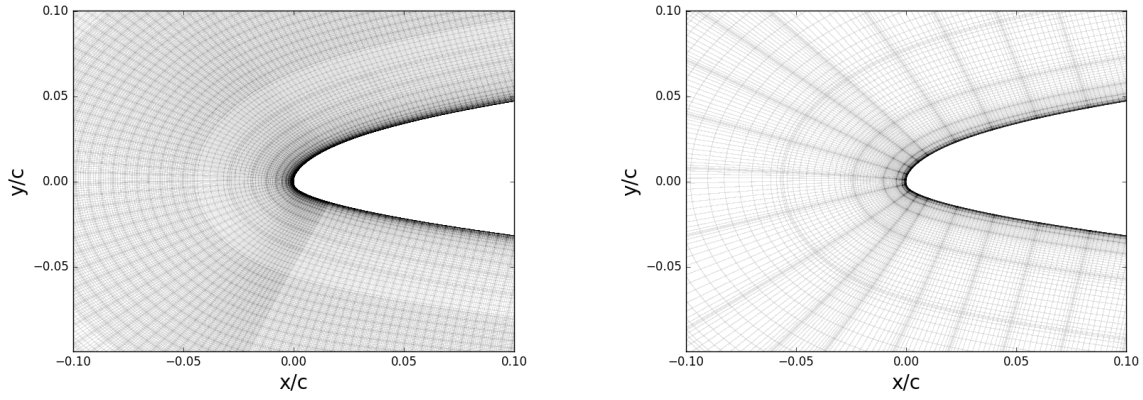

(a) New grid

(b) Old grid

Fig. 9 Close-up of the grid around the leading edge of the wing in the plane $\mathrm{x/c} = 0$.

V. Workplan

The paper will present the results of scale-resolving simulations compared to the experiments. We will investigate what types of freestream and surface disturbances may be required to activate the TS, stationary and traveling crossflow modes observed by Dagenhart and Saric. Experimental studies such as that by Downs et al on the effect of freestream turbulence on the development of cross-flow disturbances [34] will be used to guide the analysis. The inflow turbulence may for example be generated using a linear forcing technique adapted for the current DG framework [35], with an integral length scale corresponding to the low-frequency range of the freestream turbulence intensity spectrum measured in the wind tunnel. Surface roughness was suggested as a possible contributor in Ref. [22] and will therefore also be considered guided by receptivity analyses of 3D boundary layers [36]. Depending on the findings, simulations of a larger spanwise domain may be undertaken in an attempt to model the large-scale features of the transition front. Leading edge surface roughness may be generated using the methodology proposed in Ref. [31], wherein a representative roughness pattern is projected on to higher-order polynomials at the wall boundary and a high-order continuous Garlerkin approach is used to perturb the volume nodes using a linear-elasticity analogy.

References

[1] Kruse, M., Wunderlich, T., and Heinrich, L., "A conceptual study of a transonic NLF transport aircraft with forward swept wings," *30th AIAA Applied Aerodynamics Conference*, New Orleans, LA, 2012. doi:10.2514/6.2012-3208.

[2] Arthur, M., and Atkin, C., "Transition modelling for viscous flow prediction," 36th AIAA Fluid Dynamics Conference and Exhibit, 2006. doi:10.2514/6.2006-3052.

[3] Krumbein, A., Krimmelbein, N., and Schrauf, G., "Automatic Transition Prediction in Hybrid Flow Solver, Part 1: Methodology and sensitivities," *Journal of Aircraft*, Vol. 46, No. 4, 2009, pp. 1176–1190. doi:10.2514/1.39736.

[4] Langtry, R., and Menter, F., "Correlation-based transition modeling for unstructured parallelized fluid dynamics codes," *AIAA Journal*, Vol. 47, No. 12, 2009, pp. 2894–2906. doi:10.2514/1.42362.

[5] Coder, J., Pulliam, T., and Jensen, J., "Contributions to HiLiftPW-3 using structured, overset grid methods," *SciTech Forum*, 2018. doi:10.2514/6.2018-1039.

[6] Ashton, N., Denison, M., and Zastawny, M., "3rd High-Lift Workshop summary paper - OpenFOAM, STAR-CCM+ & LAVA simulations on unstructured grids," *2018 AIAA Aerospace Sciences Meeting*, 2018. doi:10.2514/6.2018-1253.

[7] Sørensen, N.N., Bechmann, A., and Zahle, F., "3D CFD computations of transitional flows using DES and a correlation based transition model," *Wind Energy*, Vol. 14, 2011, pp. 77–90. doi:10.1002/we.404.

[8] Booth, D., "A Comparison of Hybrid Reynolds-averaged Navier-Stokes/Large-Eddy Simulation (RANS/LES) and Unsteady RANS Predictions of Separated flow for a variable-speed power-turbine blade operating with low inlet turbulence levels," Tech. Rep. ARL-TR-8191, US Army Research Laboratory, October 2017.

[9] Coder, J., and Ortiz-Melendez, H., "Transitional Delayed Detached Eddy Simulation of multielement, high-lift airfoils," *2018 Applied Aerodynamics Conference, AIAA AVIATION Forum*, 2018. doi:10.2514/6.2018-2846.

[10] Li, F., and Choudhari, M., "Spatially developing secondary instabilities in compressible swept airfoil boundary layers," *Theoretical Computational Fluid Dynamics*, Vol. 25, 2011, pp. 65–84. doi:10.1007/s00162-010-0190-x.

[11] Li, F., Choudhari, M., L., D., and Chang, C.-L., "Nonlinear development and secondary instability of traveling crossflow vortices," *Physics of Fluids*, Vol. 26, No. 064104, 2014, pp. 1–19. doi:10.1063/1.4883256.

[12] Saric, W., Reed, H., and White, E., "Stability and transition of three-dimensional boundary layer," *Annual Review of Fluid Mechanics*, Vol. 35, 2003, pp. 413–440. doi:10.1146/annurev.fluid.35.101101.161045.

[13] Malik, M., Liao, W., Li, F., and Choudhari, M., "DRE-enhanced swept-wing natural flow at high Reynolds numbers," *51st AIAA Aerospace Sciences Meeting*, 2013. doi:10.2514/6.2013-412.

[14] Malik, M., Li, F., Choudhari, M., and Chang, C.-L., "Secondary instability of crossflow vortices and swept-wing boundary layer transition," *Journal of Fluid Mechanics*, Vol. 399, 1999, pp. 85–115. doi:10.1017/S0022112099006291.

[15] Mistry, V., Page, G., and McGuirk, J., "Large Eddy Simulation of crossflow vortices on an infinite swept wing," New Orleans, LA, 2012. doi:10.2514/6.2012-2694.

[16] Duan, L., Choudhari, M., and Li, F., "DNS of laminar-turbulent transition in swept-wing boundary layer," *Proceedings of the Summer Program 2014*, Stanford University, 2014, pp. 273–283.

[17] Nishino, T., and Shariff, K., "Direct numerical simulation of a swept-wing boundary layer with an array of discrete roughness elements," *7th UTAM Symposium on Laminar-Turbulent Transition*, IUTAM Bookseries, Vol. 18, Springer, Dordrecht, 2010, pp. 289–294. doi:10.1007/978-90-481-3723-7_46.

[18] Tempelmann, D., Schrader, L., Hanifi, A., Brandt, L., and Henningson, D., "Swept wing boundary-layer receptivity to localized surface roughness," *Journal of Fluid Mechanics*, Vol. 711, 2012, pp. 516–544. doi:10.1017/jfm.2012.405.

[19] Saric, W., Carrillo, R., and Reibert, M., "Nonlinear stability and transition in 3-D boundary layers," *Meccanica*, Vol. 33, No. 5, 1998, pp. 469–487. doi:10.1023/A:1004368526215.

[20] Reibert, M., Saric, W., Carrillo, R., and Chapman, K., "Experiments in nonlinear saturation of stationary crossflow vortices in a swept-wing boundary layer," *34th Aerospace Sciences Meeting and Exhibit, Aerospace Sciences Meetings*, 1996. doi:10.2514/6.1996-184.

[21] Butler, A., and Wu, X., "Stationary crossflow vortices near the leading edge of three-dimensional boundary-layers: the role of non-parallelism and excitation by surface roughness," *J. Fluid Mech.*, Vol. 845, 2018, pp. 93–140. doi:10.1017/jfm.2018.226.

[22] Dagenhart, J., and Saric, W., "Crossflow stability and transition experiments in swept-wing flow," Tech. Rep. TP-1999-209344, NASA, July 1999.

[23] Diosady, L., and Murman, S., "Design of a variational multiscale method for turbulent compressible flows," *21st AIAA Computational Fluid Dynamics Conference*, San Diego, CA, 2013. doi:10.2514/6.2013-2870.

[24] Diosady, L., and Murman, S., "Higher-order methods for compressible turbulent flows using entropy variables," *53rd AIAA Aerospace Sciences Meeting*, Kissimmee, FL, 2015. doi:10.2514/6.2015-0294.

[25] de Wiart, C., Diosady, L., Garai, A., Burgess, N., Blonigan, P., Ekelschot, D., and Murman, S., "Design of a modular monolithic implicit solver for multi-physics applications," *2018 AIAA Aerospace Sciences Meeting*, Kissimmee, FL, 2018. doi:10.2514/6.2018-1400.

[26] Murman, S., Diosady, L., Garai, A., and Ceze, M., "A space-time discontinuous-Galerkin approach for separated flows," *54th AIAA Aerospace Sciences Meeting*, San Diego, CA, 2016. doi:10.2514/6.2016-1059.

[27] Diosady, L., and Murman, S., "A linear-elasticity solver for higher-order space-time mesh deformation," *2018 AIAA Aerospace Sciences Meeting*, Kissimmee, FL, 2018. doi:10.2514/6.2018-0919.

[28] Ismail, F., and Roe, P., "Affordable, entropy-consistent Euler flux functions II: entropy production at shocks," *Journal of Computational Physics*, Vol. 228, 2009, pp. 5410–5436. doi:10.1016/j.jcp.2009.04.021.

[29] Bassi, F., and Rebay, S., *Lecture Notes in Computational Science and Engineering*, Springer, Berlin, Heidelberg, Germany, 2000, Vol. 11, Chaps. GMRES discontinuous Galerkin solution of the compressible Navier-Stokes equations, pp. 197–208. doi:10.1007/978-3-642-59721-3_14.

[30] Diosady, L., and Murman, S., "DNS of flows over periodic hills using a discontinuous Galerkin spectral-element method," *44th AIAA Fluid Dynamics Conference*, Atlanta, GA, 2014. doi:10.2514/6.2014-2784.

[31] Garai, A., Diosady, L., Murman, S., and Madavan, N., "Scale-resolving simulations of low-pressure turbine cascades with wall roughness using a spectral-element method," *ASME Turbo Exp 2018: Turbomachinery Technical Conference and Exposition*, Oslo, Norway, 2018. doi:10.1115/GT2018-75982.

[32] Ceze, M., Diosady, L., and Murman, S., "Development of a high-order space-time matrix-free adjoint solver," *54th AIAA Aerospace Sciences Meeting*, San Diego, CA, 2016. doi:10.2514/6.2016-0833.

[33] Downs, R. I., Lovig, E., and White, E., "Experimental investigation of the crossflow instability in moderate freestream turbulence," *42nd AIAA Fluid Dynamics Conference and Exhibit*, New Orleans, LA, 2012. doi:10.2514/6.2012-2824.

[34] Downs, R. I., and White, E., "Free-stream turbulence and the development of cross-flow disturbances," *Journal of Fluid Mechanics*, Vol. 735, 2013, pp. 347–380. doi:10.1017/jfm.2013.484.

[35] Garai, A., Diosady, L., Murman, S., and Madavan, N., "DNS of low-pressure turbine cascade flows with elevated inflow turbulence using a Discontinuous-Galerkin spectral-element method," *ASME. Turbo Expo: Power for Land, Sea, and Air*, Vol. Volume 2C: Turbomachinery, 2016. doi:10.1115/GT2016-56700.

[36] Schrader, L.-U., Brandt, L., and Henningson, D., "Receptivity mechanisms in three-dimensional boundary-layer flows," *Journal of Fluid Mechanics*, Vol. 618, 2008, pp. 209–241. doi:10.1017/S0022112008004345.